



Green synthesis of hyaluronic acid-silver nanoparticles using microalgae extracts, with evaluation of antimicrobial activity

Nur Imanina Abdullah Thaidi^{1,2}, Muhammad Azmirul Yusuf^{1,2}, Zahir Haizat Muhamad Zamani¹, Joo Shun Tan^{2,3}, Ahmad Badruddin Ghazali⁴, Rosfarizan Mohamad^{1,2}, Helmi Wasoh^{1,2}, Murni Halim^{1,2,*}

¹Department of Bioprocess Technology, Faculty of Biotechnology and Biomolecular Sciences, Universiti Putra Malaysia, 43400, Serdang, Selangor, Malaysia

²Bioprocessing and Biomanufacturing Research Complex, Universiti Putra Malaysia, UPM Putra InfoPort - IOI Resort, Jalan Kajang - Puchong, 43400 UPM Serdang, Selangor, Malaysia

³School of Industrial Technology, Universiti Sains Malaysia, 11800 Gelugor, Malaysia

⁴Department of Oral Maxillofacial Surgery and Oral Diagnosis, Kulliyah of Dentistry, International Islamic University Malaysia, 25200 Kuantan, Malaysia

*Corresponding author: murnihalim@upm.edu.my

SUBMITTED 19 January 2024 REVISED 23 January 2025 ACCEPTED 4 February 2025

ABSTRACT Silver nanoparticles (AgNPs) exhibit excellent antimicrobial activity but face challenges such as aggregation and reduced effectiveness when used alone. To address these limitations, green synthesis methods utilizing biological agents as reducing agents have been explored to develop AgNP nanocomposites. This study synthesized AgNPs by incorporating hyaluronic acid (HA) with microalgae extracts from *Arthrospira platensis*, *Chlorella vulgaris*, and *Nannochloropsis* sp., resulting in HA-AgNP nanocomposites. The experimental parameters, including pH, extract concentration, temperature and synthesis time, were optimized for the preparation of the HA-AgNPs nanocomposites. The best HA-AgNPs nanocomposites, synthesized by *A. platensis* (HA-SP-AgNPs), exhibited a Z-average size of 66.98 nm and polydispersity index (PDI) of 0.494, indicating uniformity and stability. FTIR analysis confirmed the presence of functional groups associated with AgNPs, HA and *A. platensis*, ensuring structural stability. A key finding of the study is that HA-SP-AgNPs demonstrated enhanced antimicrobial activity against bacteria such as *Staphylococcus aureus*, *Escherichia coli*, and *Bacillus subtilis*. Notably, the HA-SP-AgNPs were particularly effective against *S. aureus* and *E. coli* compared to AgNPs alone. The results underscore the critical role of HA in enhancing nanoparticle stability and antibacterial efficacy, positioning HA-SP-AgNPs as a promising antimicrobial agent.

KEYWORDS *A. platensis*; Antimicrobe; Green synthesis; Hyaluronic acid-silver nanoparticle

1. Introduction

Nanoparticles represent an important and rapidly growing field in modern science, encompassing various classes of materials with specific sizes and shapes, typically ranging from 1 to 100 nanometers (More et al. 2022). They can be categorized based on their size, morphology, and physicochemical properties, with each category suited to a range of applications, including medical and pharmaceutical uses (Haleem et al. 2023), cosmetics (Gupta et al. 2022), and food sciences (Singh et al. 2017).

Metal nanoparticles are commonly employed to enhance mechanical properties or provide additional functional benefits to formulations. Among them, silver nanoparticles (AgNPs) are well-known for their therapeutic and antibacterial properties. They can prevent bacterial infections by disrupting bacterial membranes and DNA,

making them effective against various inflammatory conditions and useful in wound care prior to other treatments (Yu et al. 2022). AgNPs have demonstrated antimicrobial activity against a wide range of infectious and pathogenic microorganisms, making them highly effective antimicrobial agents (Ismail et al. 2021). The antimicrobial mechanisms of AgNPs are primarily linked to their ability to interact with microbial cell membranes and intracellular components (Mikhailova 2020). However, the effectiveness of conventional antimicrobial therapies using AgNPs alone is limited due to their tendency to aggregate and their relatively low antibacterial properties. These challenges have prompted the exploration of alternative strategies, such as the development of AgNP nanocomposites, which have shown great potential in addressing these limitations.

A significant advancement of this field is the synthe-

sis of hyaluronic acid-silver nanoparticles (HA-AgNPs), where hyaluronic acid (HA) and silver ions are combined, with at least one component existing on the nanometer scale (Liang et al. 2015). HA contains an abundance of negatively charged functional groups, such as carboxyl groups, which can electrostatically interact with silver ions, enabling the formation of stable HA-AgNPs (Zhang et al. 2016). During the synthesis of nanocomposite, HA serves as both capping agent and a stabilizer, preventing nanoparticle aggregation. As a result, HA-AgNP composites exhibit enhanced properties that surpass those of the individual components (Namvar et al. 2016). Furthermore, incorporating HA with AgNPs improves their biomedical properties and biocompatibility, making them suitable for various applications (Alipoor et al. 2022; Zamboni et al. 2023).

Nanoparticles can be produced through various methods, including physical, chemical, biological, and hybrid approaches (Li et al. 2011). While physical and chemical methods enable large amounts of nanoparticle production, they often require significant energy input and involve hazardous and toxic chemicals, posing risks to both health and the environment (Sharifi-Rad et al. 2024). To mitigate these issues, an environmentally friendly alternative known as green synthesis has gained attention. Green synthesis is an eco-friendly approach that utilized biological agents such as plants, fungi, bacteria, and algae as non-toxic reducing and capping agents for nanoparticle production (Ying et al. 2022). This method is clean, cost-effective, and environmentally sustainable (Jena et al. 2014; Mahajan et al. 2019). Additionally, nanoparticles via green synthesis are biocompatible and non-toxic, making them particularly well-suited for biomedical and pharmaceutical applications (Kaliyamurthi et al. 2016; Namvar et al. 2016).

Among various biological agents, microalgae are widely used for nanoparticle production due to their ability to accumulate large quantities of metals, reduce metal ions effectively, and offer relatively low production costs (Chugh et al. 2021). Their suitability for large-scale applications further enhances their appeal. For instance, the aqueous cell extract of *Chlorella vulgaris* has been utilized as a reducing agent to synthesize AgNPs with sizes ranging from 15 nm and 47 nm (Annamalai and Nallamuthu 2016). Similarly, dried powder of *A. platensis* has been reported for the extracellular synthesis of gold, silver, and gold/silver bimetallic nanoparticles (Govindaraju et al. 2008). Microalgae often referred to as primordial microscopic plants, offer exceptional advantages as bio-factories for nanoparticle synthesis. Unlike other microorganisms, both their live and dried biomass can be employed for this purpose (Sravani et al. 2023). Furthermore, compared to larger plants, microalgae grow rapidly and require minimal nutrient, making them an efficient and sustainable choice for nanoparticle production (Jacob et al. 2021). Rashad et al. (2019) investigated the biosynthesis of AgNPs using *A. platensis* extract and demonstrated their antibacterial activity against oral pathogens.

The study revealed that AgNPs exhibited significant antibacterial activity against *Streptococcus mutans*, *Staphylococcus aureus*, and *Enterococcus faecalis*. Additionally, Ameen et al. (2020) reported the use of *A. platensis* in AgNPs synthesis and highlighted their bactericidal activity against opportunistic nosocomial pathogens of the respiratory tract.

In this study, the green synthesis method was used to produce HA-AgNPs composites, with silver salt as the precursor and microalgae extracts from *A. platensis*, *Chlorella vulgaris*, and *Nannochloropsis* as reducing agents. The synthesis process was carried out under varying conditions to achieve the desired size and shape of the nanoparticles. Optimization of several process parameters was performed using the one-factors-at-a-time (OFAT) approach to achieve the desired characteristics. The aim of this research was to optimize the factors influencing HA-AgNPs production through green synthesis and to evaluate the properties and potential antimicrobial activities of the resulting HA-AgNPs.

2. Materials and Methods

2.1. Microorganisms, materials and reagents

The dried powder forms of three microalgae, *Arthrospira platensis* (SP), *Chlorella vulgaris* (CV), and *Nannochloropsis* sp. (NC) were purchased from Algae Living (Chenderong, Malaysia). The pathogenic bacteria strains: *Escherichia coli*, *Staphylococcus aureus*, and *Bacillus subtilis* used in the antimicrobial activity study were obtained from the culture collection of the Department of Microbiology, UPM (Malaysia). Hyaluronic acid sodium salt, sourced from *Streptococcus equi*, was purchased from Sigma Aldrich (United States). The chemicals; silver nitrate (AgNO_3), sodium hydroxide (NaOH), and hydrochloric acid (HCl) were obtained from ChemAR® (Malaysia). All chemicals and reagents used were of analytical grade.

2.2. Preparation of microalgae extracts

The microalgae extracts were prepared from dried powders of three different microalgae species: *A. platensis* (SP), *C. vulgaris* (CV), and *Nannochloropsis* sp. (NC). An aliquot of 100 mL of sterile distilled water was heated to 60 °C in a 250 mL beaker. Approximately 10 g of each microalgae powder (final concentration of 100 g/L) was then added into the beaker, and the mixture was heated at 60 °C, while continuously stirred using a magnetic stirrer for 15 min. Afterward, the mixtures were cooled and centrifuged (Thermo Fisher Scientific, USA) at 1000 × g and 4 °C for 5 min. The supernatants were then filtered using Whatman No. 1 filter paper and the filtrates were stored at 4 °C for further use.

2.3. Preparation of hyaluronic acid (HA) solution

The HA solution (1.0% w/v) (Sigma Aldrich, United States) was prepared by dissolving 0.5 g of HA in 50 mL

sterile distilled water. The solution was stirred for 1 h until a homogenous mixture was obtained (Namvar et al. 2016).

2.4. Hyaluronic acid-silver nanoparticles synthesis

The methods for synthesizing HA-AgNPs were adapted from Namvar et al. (2016) and Mahdih et al. (2012). Briefly, 2 mL of microalgae extract (50 g/L), 20 mL of AgNO₃ solution (1.0 mM) (ChemAR®, Malaysia), and 20 mL of HA solution (1% w/v) were mixed in a 50 mL beaker. The ratio of AgNO₃ solution and HA solution was 1:1, while the ratio of microalgae extract to the total formulation was 1:10. The mixture was heated to 60 °C and continuously stirred with a magnetic stirrer for 1 h. The color change of the solution monitored to confirm the reduction of silver ions to AgNPs. After the synthesis was complete, the solution was cooled and stored at 4 °C for further analysis. For the optimization of synthesis parameters using OFAT approach, each specific parameter was varied in the procedure. The synthesis process of HA-AgNPs was illustrated in Figure 1, and the roles of each component in the formulation of HA-AgNP are summarized in Table 1.

2.5. Optimization of HA-AgNP Synthesis

The optimization of HA-AgNPs synthesis using OFAT approach was conducted for several parameters, including pH, concentration of microalgae extracts, temperature, and synthesis time. Three different microalgae extracts (SP, CV, and NC) were used in the synthesis process. Each nanoparticle sample was analyzed using ultraviolet-visible (UV-Vis) spectrophotometer, and color changes in the solutions were monitored. The optimal values for each parameter were selected based on the UV-Vis spectrophotometer results and color observations.

2.5.1 pH

The method outlined in Section 2.3 was followed to produce the AgNPs, while varying pH values (pH 6, 7, 8, 9, 10, 11, and 12). The optimized pH value determined from this experiment was then used to optimize the subsequent parameters.

2.5.2 Concentration of microalgae extracts

Different concentrations of each microalgae extract (25, 50, 75, and 100 g/L) were used for the synthesis of AgNPs, following the method described in Section 2.4.

2.5.3 Temperature

Three different synthesis temperatures (50, 60, and 70 °C) were tested for the synthesis of HA-AgNP composites, following the method outlined in Section 2.4.

2.5.4 Synthesis time

Three different synthesis times i.e. 0.5, 2, and 3 h were tested for the synthesis of the HA-AgNP composites, following the method outlined in Section 2.4.

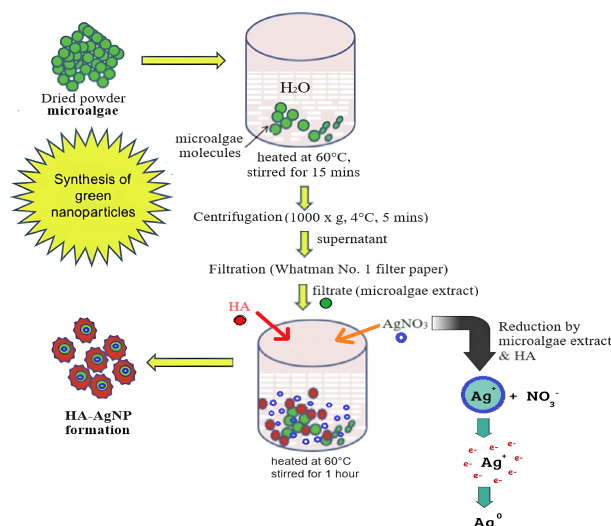


FIGURE 1 The HA-AgNPs synthesis incorporated with HA and microalgae

TABLE 1 The functions of each formulation material for the green synthesis HA-AgNPs.

Materials	Functions
Microalgae extracts	Reducing agents
Hyaluronic acid	Stabilizing, capping, and reducing agents
Silver nitrate	Source of silver ions
NaOH and HCl	For pH adjustment

2.6. Synthesis of HA-AgNP using the optimized synthesis parameters

The HA-AgNPs were synthesized using the extracts of SP, CV, and NC following the method described in Section 2.4, with the optimized parameters (pH, temperature, extract concentration, and synthesis time) determined after the OFAT optimization process. The resulting HA-AgNPs samples were characterized using UV-Vis spectrophotometer, dynamic light scattering (DLS) analysis, and Fourier transform infrared spectroscopy (FTIR).

2.6.1 UV-Vis spectroscopy analysis

UV-Vis spectroscopy analysis was conducted using a Uvi-Line 9400 spectrophotometer (Secomam, France). The wavelength range was set between 350 nm to 550 nm, with spectrum reading mode activated. A quartz cuvette with a 10 mm path length and 1 mL of HA-AgNPs solution was used for absorbance readings. If the samples absorbance reading exceeded 2.000, the samples were diluted to ensure accurate readings. Absorbance readings for each sample were performed in triplicate, and the average value was calculated.

2.6.2 DLS analysis

DLS analysis was performed using a nanoparticle sizer, Zetasizer Nano S ZEN1600 (Malvern Panalytical, United

Kingdom). The equipment was set with the following parameters: material refractive index (RI) of 0.14, dispersant (water) RI of 1.330, material absorption of 3.990, and a temperature of 25 °C. A disposable quartz cuvette with a 10 mm path length and 1 mL of sample was used for the readings. The Z-average and the polydispersity index (PDI) values for the optimized HA-AgNPs were obtained. Zetasizer software version 7.11 was used to generate the readings.

2.6.3 FTIR analysis

The chemical composition of the HA-AgNPs was analyzed using FTIR analysis (Perkin-Elmer 1725×) (Namvar et al. 2016). Prior to FTIR analysis, all samples were freeze-dried to obtain solid-form samples.

2.7. Determination of the antimicrobial activity of HA-AgNP by agar well diffusion

The antimicrobial activity of the biosynthesized SP-AgNPs and HA-SP-AgNPs was evaluated against both Gram-positive bacteria (*S. aureus* and *B. subtilis*) and a Gram-negative bacteria (*E. coli*) using the agar well diffusion method (Balouiri et al. 2016). To prepare the bacterial cultures, cell revival was performed 24 h before the experimentation day by inoculating 1% (v/v) of each pathogen in a sterile Luria-Bertani (LB) broth, followed by incubation for 24 h at 37 °C, without shaking.

For the antimicrobial test, 100 µL of each pathogenic microbial inoculum was spread evenly over the surface of a nutrient agar plate using a sterile glass spreader. The Mueller Hinton Agar (MHA) (Oxoid LTD, Basingstoke, Hampshire, GB) agar plates were allowed to rest for 30 min to dry. Then, 100 µL of test samples (controls, SP-AgNPs, HA-SP-AgNPs) were added to wells created by aseptically drilling holes (approximately 6 mm in diameter) using a micropipette tip. The agar plates were then incubated at 37 °C for 24 h. The zone of inhibition around each well was measured using a ruler, with the diameters of the inhibition zones recorded in millimeters (mm) from one edge of the zone to the opposite edge. The control used were AgNO₃, HA, and SP extracts (100 µL) and ampicillin (20 µL aliquot of 10 µg of ampicillin) was used as a positive control. The measurements were conducted in triplicate, and the mean value of the three measurements was calculated for each sample.

3. Results and Discussion

3.1. Screening of optimal parameters for synthesizing HA-AgNPs by microalgae extracts

The optimization of the HA-AgNPs green synthesis process involved adjusting four key parameters: pH, microalgae extract concentration, temperature, and synthesis time. Following the optimization, the HA-AgNP samples were analyzed using UV-Vis spectrophotometer to generate absorbance spectra across various wavelengths (nm). Surface plasmon resonance (SPR) is a phenomenon that oc-

curs when conduction electrons at the surface of metal nanoparticles interact with incident photons of a specific frequency (Saha et al. 2021). AgNPs typically exhibit SPR within a wavelength range of 350 nm to 500 nm, which corresponds to the UV-Vis absorption spectrum (Sharifi-Rad et al. 2024).

3.1.1 Effect of pH

Figure 2 presents the absorbance spectra from the UV-Vis spectrophotometer for the AgNPs synthesized using SP, CV, and NC extracts, under varying pH conditions ranging from pH 6 to pH 12. The spectra show that the SPR of AgNPs changes with increasing pH levels, regardless of the microalgae extract used. Notably, at pH 12, the highest absorption peak was observed at 410 nm for AgNPs synthesized with the SP extract (Figure 2a). The SPR peak shifted toward shorter wavelengths, transitioning from 420 nm at pH 11 to 410 nm at pH 12. This shift indicates the formation of smaller AgNP sizes, a phenomenon previously observed (Abdel-Mohsen et al. 2013). For the AgNPs synthesized with CV and NC extracts, the maximum absorption peaks were recorded at 440 nm (Figure 2b) and 430 nm (Figure 2c), respectively, both occurring at pH 11. Additionally, in both cases, the SPR intensity decreased at pH 12 after reaching its peak at pH 11. This decrease suggests that the reduction rate of silver ions was higher at pH 11 than pH 12 for both CV and NC-derived AgNPs.

It is important to note that in all three microalgae extract samples, the reduction of silver ions into AgNPs predominantly occurred under basic pH conditions. At basic pH, sodium hydroxide dissociates in water to release negatively charged hydroxide ions, which facilitate the complete reduction of silver ions into AgNPs (Traiwatcharanon et al. 2015). Therefore, the optimal pH selected for the AgNP sample from SP was pH 12, while pH 11 was chosen for the AgNPs from CV and NC.

3.1.2 Effect of microalgae extract concentration

Figure 3 presents absorbance spectra obtained from UV-Vis spectrophotometer for all three AgNPs synthesized using varying concentrations (25, 50, 75, and 100 g/L) of microalgae extracts (SP, CV, and NC).

As shown in Figure 3a, the highest absorption peak at 410 nm was observed when a 50 g/L concentration of SP extract was used for the AgNP synthesis. The intensity of the SPR increased with the concentration of microalgae extracts up to 50 g/L, after which it began to decline, accompanied by a shift towards longer wavelengths. In Figure 3b, the highest absorption peak at 450 nm was occurred with a 25 g/L concentration of CV extract. The SPR intensity of AgNP decreased as the concentration of CV extract increased, with the SPR peak shifting towards longer wavelengths. This shift suggests potential agglomeration or the formation of larger nanoparticles. Particle aggregation causes the SPR to shift to a lower energy level, resulting in longer wavelengths (Saha et al. 2021). This effect

occurs due to the delocalization and sharing of conduction electrons near the surface of individual particles, which

extends to neighboring particles. In contrast, the SPR intensity of AgNP increased with higher concentrations of

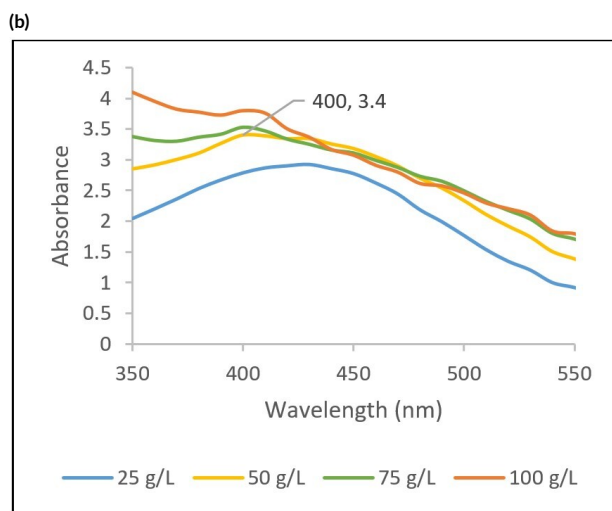
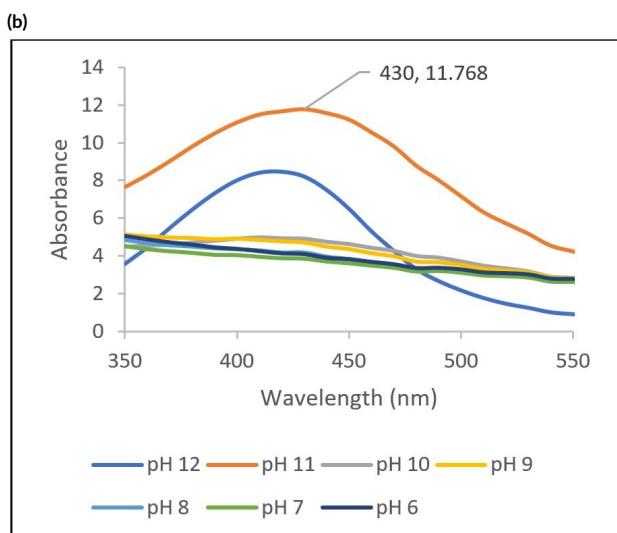
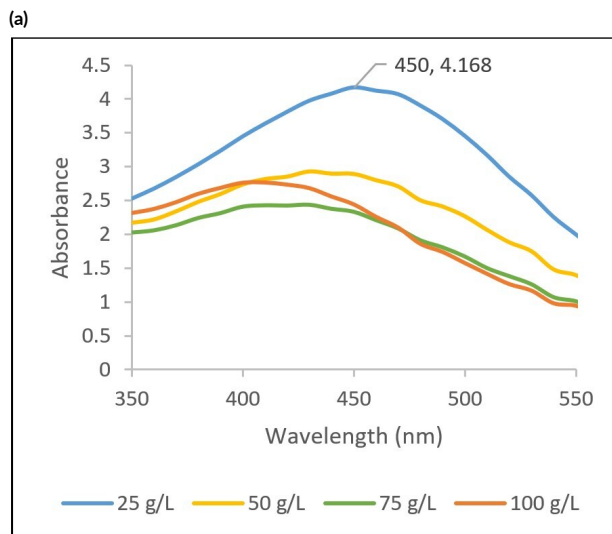
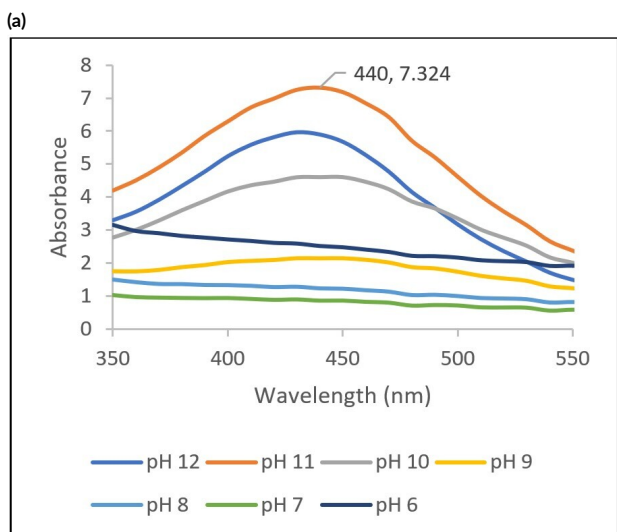
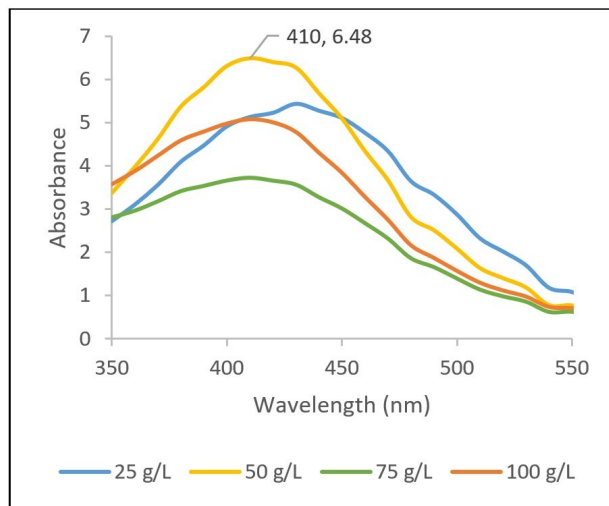
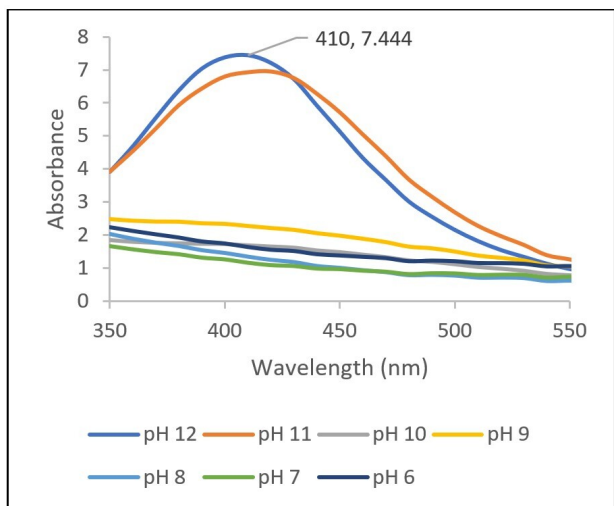


FIGURE 2 The UV-Vis spectroscopy for AgNP samples synthesized at different pH (6, 7, 8, 9, 10, 11, 12) using: (A) SP. (B) CV. (C) NC.

FIGURE 3 The UV-Vis spectroscopy for AgNPs synthesized with different concentrations (25, 50, 75, and 100 g/L) of microalgae extracts: (A) SP. (B) CV. (C) NC.

NC extract (Figure 3c). However, when the extract concentration exceeded 25 g/L, fluctuations in the absorption peaks were observed. The solution did not visibly darken, which may suggest aggregation or a reduced rate of silver ion reduction. The 25 g/L extract concentration yielded the optimal SPR peak for AgNPs synthesized by NC extract, characterized by a clear bell-shaped peak at 430 nm.

Theoretically, higher concentrations of microalgae extracts provide more biomolecules, which act as reducing agents to promote the rapid reduction of silver ions into AgNP (Saha et al. 2021). However, an excess of reducing agents can lead to aggregation due to the rapid reduction and growth of AgNP before the capping process is adequately completed. This may explain the lower SPR peaks observed at high concentrations of microalgae extracts. Based on these results, the optimal extract concentrations were determined to be 50 g/L for SP, and 25 g/L for both CV and NC extracts.

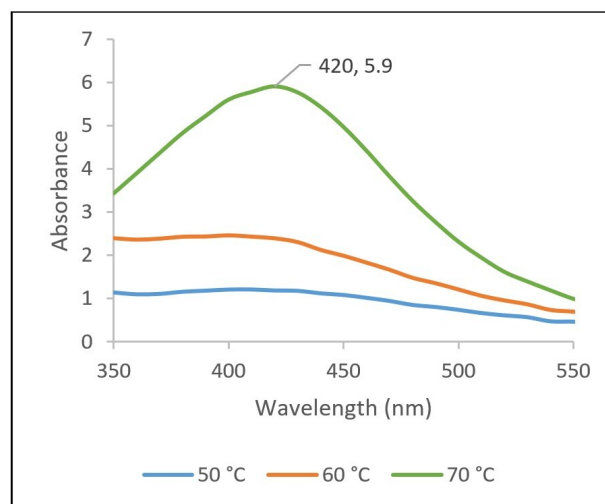
3.1.3 Effect of temperature

Figure 4 presents the UV-Vis absorbance spectra for the three HA-AgNPs synthesized using SP, CV, and NC extracts at three different synthesis temperatures: 50°C, 60°C, and 70°C. A key feature of the spectra is the maximum SPR peaks, which were observed in the wavelength range of 400 - 430 nm.

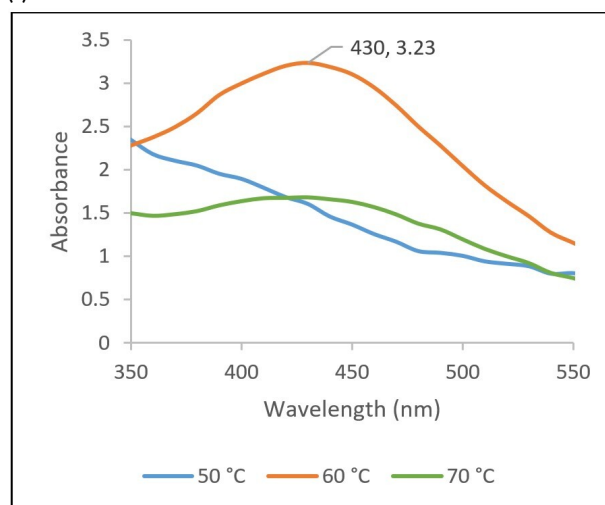
As shown in Figure 4a, increasing the synthesis temperature for HA-AgNPs using SP extract resulted in a significant rise in SPR intensity. The highest absorption peak, at 420 nm, was achieved at 70°C. This enhanced SPR intensity suggests a more rapid reduction of silver ions at elevated temperatures, which can be attributed to accelerated reaction rates and increased atomic mobility in the solution (He et al. 2024). These conditions promote the formation of smaller nanoparticles with a narrower size distribution.

In contrast, as depicted in Figure 4b, the SPR intensity of HA-AgNPs synthesized by CV extract increased with rising temperatures but declined when the temperature exceeded 60°C. The maximum absorption peak was observed at 430 nm at 60°C. However, temperatures above 60°C appeared to initiate gradual degradation of the HA component, potentially compromising the stability of the HA-AgNP composite (Mondek et al. 2015). This degradation likely explains the decreased SPR intensity observed at 70°C for the HA-AgNP of CV extract samples. Similarly, for HA-AgNP synthesized using NC extract, the highest absorption peak was recorded at 400 nm when the temperature was maintained at 60°C, as shown in Figure 4c. The SPR intensity increased with temperature but declined beyond 60°C. Moreover, the SPR peaks exhibited a notably flat curve for all HA-AgNP of NC extract samples. Based on these findings, the optimal temperature for SP is 70°C, while 60°C is most suitable for CV and NC extract samples. This conclusion is drawn from the observed SPR intensity, as well as considerations of HA stability and its influence on nanocomposite forma-

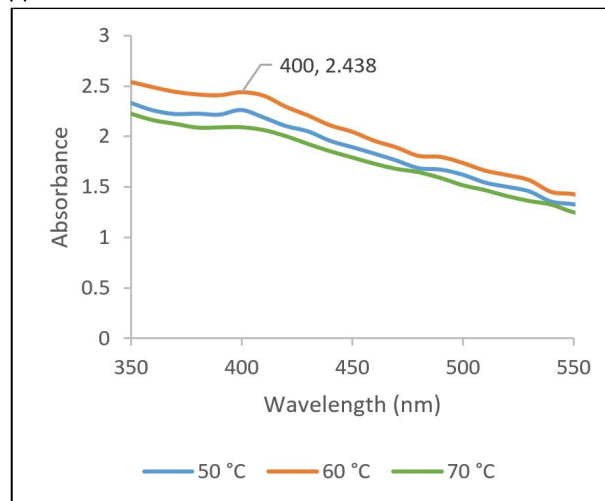
tion.



(a)

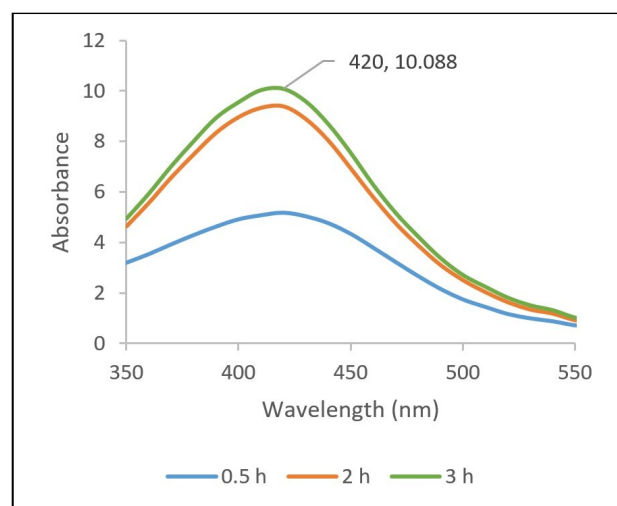


(b)

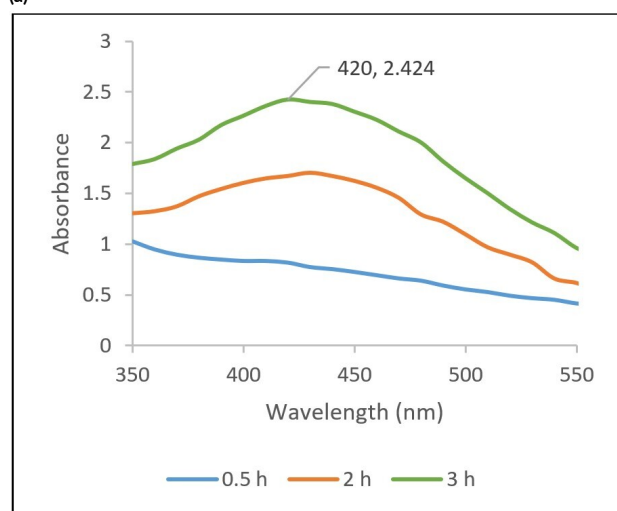


(c)

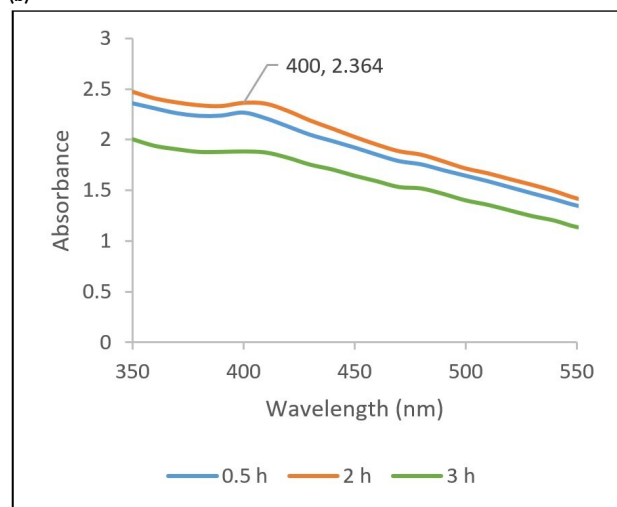
FIGURE 4 The UV-Vis spectroscopy for HA-AgNP composite synthesized at different temperatures (50, 60, and 70°C) using: (A) SP. (B) CV. (C) NC.



(a)



(b)



(c)

FIGURE 5 The UV-Vis spectroscopy for HA-AgNPs synthesized at different synthesis times (0.5, 2, 3 h), at 60°C using: (A) SP. (B) CV. (C) NC.

3.1.4 Effect of synthesis time

Figure 5 presents the UV-Vis spectra for the three HA-AgNPs synthesized using SP, CV and NC extracts at various synthesis durations: 0.5, 2, and 3 h.

As shown in Figure 5a, the SPR intensity of HA-AgNP synthesized using SP extract increased with longer synthesis times, reaching its maximum at 420 nm after 3 h of incubation. Prolonged incubation time allows greater interaction between the reducing agents and silver ions, facilitating more efficient conversion into AgNPs (Vadakkan et al. 2024). However, further incubation beyond this period had no significant affect on the synthesis rate. Similarly, Figure 5b shows that the SPR intensity of HA-AgNP synthesized with CV extract also increased with longer synthesis time, with the maximum absorption peak observed at 420 nm after 3 h. This finding alignes with documented evidence that HA can serve as both a stabilizer and a reducing agent during AgNP biosynthesis, contributing to its effectiveness in nanoparticle formation (Hussein and Abdullah 2022).

In contrast, Figure 5c, indicates that HA-AgNP synthesized with NC extract exhibited a maximum absorption peak at 400 nm for a 2-hour incubation period. Although the SPR intensity increased with incubation time, it declined beyond 2 h. This decline is likely due to the potential aggregation of AgNPs during extended incubation, which can negatively impact SPR intensity (Vadakkan et al. 2024). Furthermore, the relatively flat SPR peaks observed for HA-AgNP of NC extract suggest less efficient reduction of silver ions into AgNP. Based on these results, the optimal synthesis time for HA-AgNPs from SP and CV extracts was determined to be 3 h, while a 2-hour was identified as the optimal duration for HA-AgNPs from NC extract.

3.2. Effect of integrating HA and microalgae extracts in synthesizing HA-AgNP under optimized parameters

3.2.1 Synthesis of HA-AgNP with optimized parameters

The synthesis of HA-AgNP composites using three microalgae extracts, SP, CV, and NC, was further investigated under optimized reaction conditions to evaluate the effects of pH, extract concentration, temperature, and synthesis time on the resulting nanoparticles (Section 3.1).

Figure 6 illustrates the UV-Vis spectra of HA-AgNP synthesized using the optimized parameter values. The highest absorption peak was observed for HA-AgNP synthesized with SP extract, occurring at 410 nm (Figure 6a). This sharp and well-defined SPR peak indicates the production of relatively small and uniform AgNPs. The high absorption intensity at this wavelength signifies efficient reduction and stabilization of silver ions by SP extract (Saha et al. 2021). These results align with previous studies that highlight the potential of SP as an effective reducing agent and stabilizer for AgNP synthesis (Ismail et al. 2021).

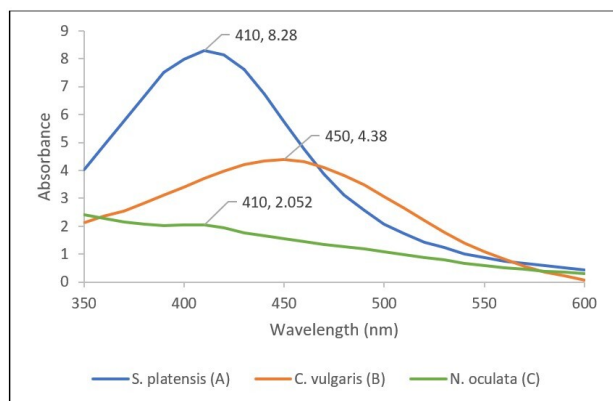


FIGURE 6 UV-Vis spectra for HA-AgNPs synthesized under the optimized parameters using A. SP. ,B. CV.,C. NC.

In contrast, the UV-Vis spectrum of HA-AgNP synthesized using CV extract showed a decrease in SPR intensity and a redshift of the peak to approximately 450 nm (Figure 6b). This shift suggests the formation of larger AgNPs. The variation in SPR peak characteristics with CV extract may be due to differences in the reducing and stabilizing capabilities of the algae extract, resulting in the production of nanoparticles with larger sizes. Meanwhile, the HA-AgNPs synthesized using NC exhibited the lowest absorption intensity, with the peak also appearing at 410 nm (Figure 6c). However, the SPR peak in this spectrum was relatively flat and lacked the characteristic bell-shaped curve seen in the other spectra. This result indicates that the reduction process of silver ions by this formulation was likely inefficient, producing a low concentration of AgNPs.

The UV-Vis spectroscopic analysis of HA-AgNPs synthesized from the three different microalgae extracts revealed distinct variations in SPR peak characteristics, reflecting differences in nanoparticle size, uniformity, and stability. SP extract demonstrated the greatest efficacy in producing smaller, more uniform HA-AgNPs with a well-defined SPR peak compared to the sHA-AgNPs synthesized using CV and NC extracts.

3.2.2 Observation of color change on HA-AgNP synthesis

Table 2 summarizes the visual observations of the optimized HA-AgNP synthesized using three different microalgae extract solutions, both before and after the synthesis process. During synthesis, where the mixture was heated to a specific temperature, silver ions were gradually reduced by the biological molecules in the microalgae extracts to form HA-AgNPs. The observed color change to dark brown was attributed to the SPR of AgNP, indicating successful nanoparticle formation (Murugan et al. 2014).

According to Table 2, the initial color of the synthesis mixtures with SP and CV extracts transformed to dark brown by the end of the synthesis process, confirming the characteristic SPR and the successful formation of HA-

TABLE 2 The color change of the HA-AgNP mixture during the synthesis using optimized parameters.

HA- AgNP	Before synthesis	After synthesis
<i>A. platensis</i> (SP)		
<i>C. vulgaris</i> (CV)		
<i>Nannochloropsis</i> (NC)		

AgNPs. In contrast, the color of the synthesis mixture using NC extract remained unchanged. This suggests either a very low concentration of AgNPs or poor formation. A potential explanation for this observation is that the interactions between the components in the NC solution may have interrupted the process, resulting in a slower reduction of silver ions into HA-AgNPs (Vadakkan et al. 2024).

3.2.3 DLS analysis

DLS is used to determine the hydrodynamic size of particles based on the mechanism of light scattering as photons travel through a colloidal solution. The Z-average obtained from the DLS analysis represents the average size (d.nm) of nanoparticles in the sample, while the polydispersity index (PDI) indicates the size distribution of the particles. A low PDI value reflects good quality and uniformity of nanoparticles (More et al. 2022).

Table 3 presents the results of the DLS analysis for the optimized HA-AgNPs synthesized using SP, CV, and NC extracts. For HA-SP-AgNP synthesized using SP extract, the Z-average was 66.98 nm, and the PDI value was 0.494. A PDI values below 0.5 is generally considered acceptable for nanoparticles containing polymers (Ferreira-Gonçalves et al. 2022). In contrast, HA-CV-AgNP and HA-NC-AgNP synthesized from CV and NC extracts exhibited very high Z-average values (5677 nm and 2928 nm, respectively) and highly polydisperse PDI (both 1.000). These results suggest that the nanoparticles formed using CV and NC extracts were significantly larger and less uniform compared to those synthesized with SP extract. The synthesis of HA-SP-AgNP demonstrated promising results, with an average particle size below 100 nm, surpassing the performance of both HA-CV-AgNP and HA-

TABLE 3 The results of DLS analysis for the optimized synthesis of HA/AgNP composites.

HA/AgNP	Z-Average (d.nm)	DPI
HA-SP-AgNP	66.98 ± 0.015	0.494 ± 0.01
HA-CV-AgNP	5677 ± 0.03	1.00 ± 0.05
HA-NC-AgNP	2928 ± 0.5	1.00 ± 0.1

NC-AgNP. This size advantage highlights the superior potential of HA-SP-AgNP, making it the most suitable candidate for further investigation.

3.3. Comparison between HA-SP-AgNP and SP-AgNP

3.3.1 Comparative evaluation on characterization of HA-SP-AgNP and SP-AgNP

This study provides a detailed characterization and comparison of two types of AgNPs synthesized using SP extract: AgNP incorporated with HA (HA-SP-AgNP) and AgNPs synthesized without the addition of HA (SP-AgNP). Both types of AgNPs were prepared using the previously established method (Section 3.2.1). Key parameters, including UV-Vis spectra, color changes during synthesis, Z-average, and PDI were analyzed and compared to highlight their differences and assess their potential applications (Table 4).

TABLE 4 Comparison of characterization of HA-SP-AgNP and SP-AgNP.

Characterization	HA-SP-AgNP	SP-AgNP
UV-vis	410 nm, peak 8.28	405 nm, peak 1.87
Color change during synthesis	Green to dark brown	Green to dark brown
Z-average	66.98 ± 0.025	137.33 ± 13
PDI	0.494 ± 0.05	0.506 ± 0.01

It was observed that HA-SP-AgNP exhibited a peak at 410 nm with an absorbance reading of 8.28, while SP-AgNP displayed a peak at 405 nm with a lower absorbance reading of 1.87. This indicates that HA-SP-AgNP has a higher absorbance at a slightly longer wavelength compared to SP-AgNP. The differences in UV-Vis spectra between the two nanoparticles may be attributed to variations in their synthesis methods or the presence of distinct capping agents either HA and SP or SP alone. Both HA-SP-AgNP and SP-AgNP underwent a visible color change from green to dark brown during synthesis, a transformation commonly associated with the reduction of silver ions to AgNP and indicative of successful nanoparticle formation.

The HA-SP-AgNP demonstrated a Z-average of 66.98 ± 0.025 nm, while SP-AgNP had a larger Z-average size of 137.33 ± 13 nm. This suggests that HA-SP-AgNP particles are smaller and more uniformly dispersed compared to SP-AgNP. The smaller size of HA-SP-AgNP can be attributed to the dual action of HA and SP extract as capping agents, which likely enhanced control over nanoparticle growth and aggregation during synthesis. This highlights the critical role of HA in modulating particle size and distribution.

Additionally, the HA-SP-AgNP exhibited a dispersity (PDI) of 0.494 ± 0.05, while was slightly lower than the 0.506 ± 0.01 dispersity of SP-AgNP. The lower PDI of HA-SP-AgNP indicates uniformity and a higher degree of monodispersed compared to SP-AgNP. A lower PDI reflects a more homogenous particle size distribution, mean-

ing that the particles in the sample are more uniform in size (More et al. 2022).

The incorporation of HA in the synthesis of AgNP provide several advantages, emphasizing its role in enhancing the nanoparticle stability, biocompatibility, and potential applications. One of the key benefits of using HA is its ability to improve nanoparticle stability. HA, a high molecular weight polysaccharide, contains multiple functional groups, such as carboxyl and hydroxyl groups (Hintze et al. 2022), that bind effectively to the surface of AgNP. These functional groups serve as capping agents, preventing agglomeration and subsequent precipitation of the nanoparticles. This enhanced stability is crucial for the long-term storage and broader application of AgNP.

3.3.2 Comparative evaluation of antimicrobial activity of HA-SP-AgNP and SP-AgNP

The antimicrobial activity of HA-SP-AgNP and SP-AgNP against three pathogenic bacterial strains; *S. aureus*, *E. coli*, and *B. subtilis* was accessed using the zone of inhibition (ZOI) by the agar well diffusion assay (Table 5).

HA-SP-AgNP exhibited a significantly larger ZOI against *S. aureus* compared to SP-AgNP, with ZOIs of 15.10 mm and 13.93 mm, respectively. This results indicates superior antimicrobial activity of HA-SP-AgNP against the *S. aureus* strain. For *B. subtilis*, both HA-SP-AgNP and SP-AgNP demonstrated comparable ZOI (9.33 mm and 9.67 mm, respectively). Interestingly, SP-AgNP showed no inhibitory effect against *E. coli*, whereas HA-SP-AgNP displayed a ZOI of 10 mm suggesting it has a broader antimicrobial spectrum. The lack of activity in some cases may reflect the inherent resistance mechanisms of certain bacterial strains against silver nanoparticles, and it is also possible that the addition of microalgae extract alone does not significantly enhance the antimicrobial activity against resistant strains (Hanisha et al. 2024). These findings emphasize the advantage of incorporating HA as a capping agent, as it broadens the antimicrobial activity, particularly against *E. coli*. Previous studies have demonstrated the remarkable antimicrobial efficacy of HA-AgNP against *S. aureus* and *E. coli*, often depending on nanoparticle size (Abdel-Mohsen et al. 2013). Furthermore, HA provides a biocompatible coating, making the nanoparticles suitable for diverse medical applications, including drug delivery, wound healing, and tissue engineering (Liang et al. 2015). The inclusion of HA not only enhances the stability of AgNP but also reduces the cytotoxicity, improving compatibility with biological systems (Hussein and Abdullah 2022).

Ampicillin, used as a positive control, exhibited moderate antimicrobial activity against all three pathogenic bacterial strains. Interestingly, HA-SP-AgNP demonstrated greater antimicrobial activity against *S. aureus*, *B. subtilis*, and *E. coli* compared to ampicillin, highlighting its potential as an alternative or complementary antimicrobial agent to conventional antibiotics. In a separate control study, AgNO₃, which releases silver ions, exhibited antimicro-

TABLE 5 The zone of inhibition (in mm) by agar well diffusion assay for antimicrobial activity of HA-SP-AgNP and SP-AgNP.

Antimicrobial activity	Zone of Inhibition (mm)		
	<i>S. aureus</i>	<i>B. subtilis</i>	<i>E. coli</i>
HA-SP-AgNP	15.10 ± 0.2 ^a	9.33 ± 0.25 ^a	10 ± 0.23 ^a
SP-AgNP	13.93 ± 0.31 ^b	9.67 ± 0.4 ^a	0
Ampicillin (control)	11±0.23 ^c	6.5 ± 0.3 ^b	7 ± 0.5 ^b
AgNO ₃ (control)	10±0.18 ^d	0	10 ± 0.5 ^a
HA (control)	0	0	0
SP extract (control)	0	0	0

Note: The results are expressed as mean (n = 3) ± SD. The values with different lowercase letters within the same column are significantly different (p < 0.05).

bial activity against *S. aureus* and *E. coli* but not against *B. subtilis*. This suggests that the antimicrobial effects of HA-SP-AgNP and SP-AgNP are likely attributed to a combination of silver ions and the stabilizing agents.

Control tests using HA and SP extracts alone did not show any antimicrobial activity, indicating that the observed effects are primarily due to the nanoparticles or nanocomposites. However, previous research by Shuai et al. (2021) explored the antimicrobial properties of HA and found it effective effects against various pathogens, including *S. aureus* and *E. coli*. While the precise mechanisms remain under investigation, it is hypothesized that the negatively charged carboxyl and sulfate groups in HA interact with bacterial cell walls, disrupting their structural integrity (Zamboni et al. 2023). Further studies are needed to elucidate these mechanisms, as the antimicrobial potential could be harnessed to develop novel antimicrobial agents or coatings for medical devices, reducing infections risks in healthcare settings.

Moreover, HA possesses intrinsic antioxidant properties due to its ability to scavenge free radicals (Ke et al. 2011). When combined with AgNP, which also exhibits antioxidant activity, a synergistic effect may enhance the overall antioxidant capacity of the composite. This synergy could make HA-AgNP valuable in applications targeting oxidative stress and inflammation.

3.4. FTIR analysis

FTIR spectroscopy is a powerful analytical technique used to identify and analyze the chemical composition of materials by measuring the absorption of infrared radiation by their molecular bonds. In this study, FTIR spectra were obtained for HA-SP-AgNP, SP extract, and HA standard to verify the chemical composition and confirm the successful formation of the HA-SP-AgNP composite (Figure 7).

For the HA standard, several absorption peaks were observed at 428 cm⁻¹, 459 cm⁻¹, 531 cm⁻¹, 560 cm⁻¹, 591 cm⁻¹, and 611 cm⁻¹, corresponding to the characteristic vibrational modes of HA molecules (Sravani et al. 2023). The peaks represents the molecular vibrations associated with HA. Notably, a peak at 1398 cm⁻¹ observed in the HA standard was also detected in the HA-SP-AgNP composite, confirming the presence of HA in the composite.

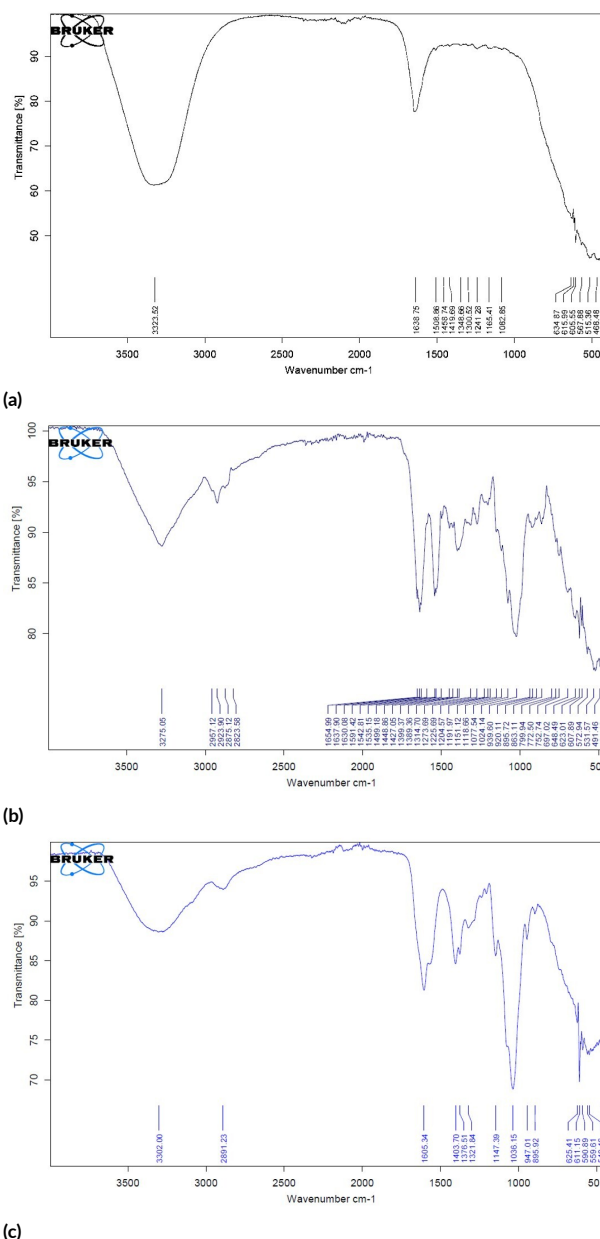


FIGURE 7 FTIR spectra of, (A) HA-SP-AgNP. (B) SP extract. (C) HA standard.

TABLE 6 The peak number and their positions (cm^{-1}) of FTIR spectroscopy of HA-SP-AgNP, SP, HA standard, and AgNP (from published reports).

Peak No.	FTIR Wavenumber Peak (cm^{-1})				
	HA/AgNP	*HA	^a AgNP	^b AgNP	^c AgNP
1	441	-	-	-	-
2	468	459	-	-	-
3	515	-	-	-	-
4	567	560	-	-	-
5	605	591	-	-	-
6	615	611	-	-	-
7	635	-	-	-	-
8	1082	-	-	1051	1020
9	1165	1147	-	1148	-
10	1241	-	-	1237	1220 (1200-1300)
11	1300	1322	-	-	-
12	1349	1377	-	-	-
13	1418	1404	1383	1398	-
14	1458	-	-	1448	1448
15	1508.86	-	-	-	-
16	1638	-	1631	1637	1640
17	-	2891	2927	-	-
18	3323	3302	-	-	3100-3400

Note: *HA standard, Published studies of AgNP from: ^a(Devaraj et al. 2013), ^b(Kaliyamurthi et al. 2016), and ^c(Pandian et al. 2015).

Additionally, a broad absorption region was noted in the 3100–3400 cm^{-1} range, with peaks at 3323 cm^{-1} for HA-SP-AgNP and 3275 cm^{-1} for SP indicating O-H stretching vibrations, typical of hydroxyl groups in organic compounds (Salgin et al. 2017). The similarity of these peaks across samples, suggests shared chemical bonds or structural elements in HA-SP-AgNP and SP.

FTIR data for HA-SP-AgNP composite, HA, and AgNP, were compared based on wavenumber peak (cm^{-1}) (Table 6). Peaks associated with AgNP were identified from previously published studies. A strong set of peaks between 1631–1640 cm^{-1} (peak 16) in the HA-SP-AgNP spectrum is attributed to the vibrational modes of AgNP. These peaks are often associated with metal-metal or metal-ligand vibrations, likely involving Ag-N or Ag-O bonds, suggesting the interactions between HA and AgNP during the synthesis process (Devaraj et al. 2013). Other peaks observed in the HA-SP-AgNP such as those at 1077 cm^{-1} , 1225 cm^{-1} , and 1404 cm^{-1} , correspond to peaks previously reported for AgNP and were also present in the composite.

A prominent peak 8 indicates the presence of functional groups or chemical bonds associated with the AgNP. This could be related to the bonding of silver atoms in the nanoparticles or surface functionalization (Kaliyamurthi et al. 2016). Another peak such as 1148 cm^{-1} (Peak 9) indicates additional chemical features in the nanoparticles, potentially related to surface modifications or ligand interactions (Kaliyamurthi et al. 2016). Peaks at 1148 cm^{-1} and 1638 cm^{-1} , are common among AgNP, HA, and HA-SP-AgNP (Pandian et al. 2015). These may represent shared

chemical bonds or functional groups in these materials.

The peaks at 441 cm^{-1} , 515 cm^{-1} , and 635 cm^{-1} were observed exclusively in HA-SP-AgNP, indicating the formation of new interactions or chemical bonds between HA and AgNP. These unique peaks may result from HA molecules adsorbing onto the AgNP surface, altering the vibrational modes of both components. The FTIR spectrum of HA-SP-AgNP exhibits a combination of peaks characteristic of both HA and AgNP, confirming the successful formation of the HA-SP-AgNP composite. This analysis demonstrates the incorporation of functional groups from both HA and SP into the nanocomposite, supporting its potential for applications requiring stable and functionalized nanoparticles.

4. Conclusions

The optimization of key experimental parameters, including pH, extract concentration, temperature, and synthesis time was pivotal in the successful development of the HA-SP-AgNP nanocomposite. The incorporation of HA and *A. platensis* significantly contributed to achieving a stable composite with a Z-Average particle size of 66.98 nm and a PDI of 0.494, indicating a uniform size distribution. FTIR analysis confirmed the successful integration of functional groups, which contributed to the structural stability of the nanocomposite. The HA-SP-AgNPs exhibited enhanced antimicrobial activity, particularly against *S. aureus* and *E. coli*, highlighting its potential as an effective antimicrobial agent. These findings underscore the

critical role of HA as a capping agent in stabilizing the nanoparticles and the contribution of silver ions to antimicrobial efficacy. Further research is needed to investigate the underlying mechanisms driving the antimicrobial and structural properties of HA-SP-AgNP, as well as its safety and potential applications in clinical settings. This study lays a strong foundation for the development of HA-SP-AgNP as a versatile nanomaterial with promising applications in antimicrobial therapies and beyond.

Acknowledgments

The research was supported by Ministry of Higher Education Malaysia through Fundamental Research Grant Scheme: FRGS/1/2019/STG05/UPM/02/30.

Authors' contributions

NIAT, MAY, ZHMZ, MH, RM, HW, JST designed the study. NIAT, MAY, ZHMZ carried out the laboratory work. NIAT, MAY, ZHMZ, MH analyzed the data. NIAT, ABG, MH wrote the manuscript. All authors read and approved the final version of the manuscript.

Competing interests

The authors declare no competing interest.

References

- Abdel-Mohsen AM, Hrdina R, Burgert L, Abdel-Rahman RM, Hašová M, Šmejkalová D, Kolář M, Pekar M, Aly AS. 2013. Antibacterial activity and cell viability of hyaluronan fiber with silver nanoparticles. *Carbohydr. Polym.* 92(2):1177–1187. doi:10.1016/j.carbpol.2012.08.098.
- Alipoor R, Ayan M, Hamblin MR, Ranjbar R, Rashki S. 2022. Hyaluronic acid-based nanomaterials as a new approach to the treatment and prevention of bacterial infections. *Front. Bioeng. Biotechnol.* 10:913912. doi:10.3389/fbioe.2022.913912.
- Ameen F, Abdullah MM, Al-Homaidan AA, Al-Lohedan HA, Al-Ghanayem AA, Almansob A. 2020. Fabrication of silver nanoparticles employing the cyanobacterium *Spirulina platensis* and its bactericidal effect against opportunistic nosocomial pathogens of the respiratory tract. *J. Mol. Struct.* 1217:128392. doi:10.1016/j.molstruc.2020.128392.
- Annamalai J, Nallamuthu T. 2016. Green synthesis of silver nanoparticles: Characterization and determination of antibacterial potency. *Appl. Nanosci.* 6(2):259–265. doi:10.1007/s13204-015-0426-6.
- Balouiri M, Sadiki M, Ibensouda SK. 2016. Methods for *in vitro* evaluating antimicrobial activity: A review. *J. Pharm. Anal.* 6(2):71–79. doi:10.1016/j.jpha.2015.11.005.
- Chugh D, Viswamalya VS, Das B. 2021. Green synthesis of silver nanoparticles with algae and the importance of capping agents in the process. *J. Genet. Eng. Biotechnol.* 19(1):126. doi:10.1186/s43141-021-00228-w.
- Devaraj P, Kumari P, Aarti C, Renganathan A. 2013. Synthesis and characterization of silver nanoparticles using cannonball leaves and their cytotoxic activity against MCF-7 cell line. *J. Nanotechnol.* 2013:598328. doi:10.1155/2013/598328.
- Ferreira-Gonçalves T, Gaspar MM, Coelho JM, Marques V, Viana AS, Ascensão L, Carvalho L, Rodrigues CM, Ferreira HA, Ferreira D, Reis CP. 2022. The role of rosmarinic acid on the bioproduction of gold nanoparticles as part of a photothermal approach for breast cancer treatment. *Biomolecules* 12(1):71. doi:10.3390/biom12010071.
- Govindaraju K, Basha SK, Kumar VG, Singaravelu G. 2008. Silver, gold and bimetallic nanoparticles production using single-cell protein (*Spirulina platensis*) Geitler. *J. Mater. Sci.* 43(15):5115–5122. doi:10.1007/s10853-008-2745-4.
- Gupta V, Mohapatra S, Mishra H, Farooq U, Kumar K, Ansari MJ, Aldawsari MF, Alalaiwe AS, Mirza MA, Iqbal Z. 2022. Nanotechnology in cosmetics and cosmeceuticals—A review of latest advancements. *Gels* 8(3):173. doi:10.3390/gels8030173.
- Haleem A, Javaid M, Singh RP, Rab S, Suman R. 2023. Applications of nanotechnology in medical field: a brief review. *Glob. Heal. J.* 7(2):70–77. doi:10.1016/j.glohj.2023.02.008.
- Hanisha R, Balaganapathy M, Eswar B, Kathirvelan P, Rajabathar J, Siddiqui N, Dinakarkumar Y. 2024. Biogenic synthesis of silver nanoparticles using *Spirulina maxima* extract and their bactericidal activity. *J. Umm Al-Qura Univ. Appl. Sci.* doi:10.1007/s43994-024-00203-4.
- He W, Liu F, Tan L, Huang L, He S, Zhang L, Fan C. 2024. Investigation on different additions as candidates for nano-oxide particles in nickel-based ODS superalloys. *Mater. Charact.* 209:113648. doi:10.1016/j.matchar.2024.113648.
- Hintze V, Schnabelrauch M, Rother S. 2022. Chemical modification of hyaluronan and their biomedical applications. *Front. Chem.* 10:830671. doi:10.3389/fchem.2022.830671.
- Hussein HA, Abdullah MA. 2022. Novel drug delivery systems based on silver nanoparticles, hyaluronic acid, lipid nanoparticles and liposomes for cancer treatment. *Appl. Nanosci.* 12(11):3071–3096. doi:10.1007/s13204-021-02018-9.
- Ismail GA, El-Sheekh MM, Samy RM, Gheda SF. 2021. Antimicrobial, antioxidant, and antiviral activities of biosynthesized silver nanoparticles by phyco-biliprotein crude extract of the Cyanobacteria *Spirulina platensis* and *Nostoc linckia*. *Bionanoscience* 11(2):355–370. doi:10.1007/s12668-021-00828-3.
- Jacob JM, Ravindran R, Narayanan M, Samuel SM,

- Pugazhendhi A, Kumar G. 2021. Microalgae: A prospective low cost green alternative for nanoparticle synthesis. *Curr. Opin. Environ. Sci. Heal.* 20:100163. doi:10.1016/j.coesh.2019.12.005.
- Jena J, Pradhan N, Nayak RR, Dash BP, Sukla LB, Panda PK, Mishra BK. 2014. Microalga *Scenedesmus* sp.: A potential low-cost green machine for silver nanoparticle synthesis. *J. Microbiol. Biotechnol.* 24(4):522–533. doi:10.4014/jmb.1306.06014.
- Kaliamurthi S, Selvaraj G, Çakmak ZE, Çakmak T. 2016. Production and characterization of spherical thermostable silver nanoparticles from *Spirulina platensis* (Cyanophyceae). *Phycologia* 55(5):568–576. doi:10.2216/15-98.1.
- Ke C, Sun L, Qiao D, Wang D, Zeng X. 2011. Antioxidant activity of low molecular weight hyaluronic acid. *Food Chem. Toxicol.* 49(10):2670–2675. doi:10.1016/j.fct.2011.07.020.
- Li X, Xu H, Chen ZS, Chen G. 2011. Biosynthesis of nanoparticles by microorganisms and their applications. *J. Nanomater.* 2011:1–16. doi:10.1155/2011/270974.
- Liang J, Zeng F, Zhang M, Pan Z, Chen Y, Zeng Y, Xu Y, Xu Q, Huang Y. 2015. Green synthesis of hyaluronic acid-based silver nanoparticles and their enhanced delivery to CD44+ cancer cells. *RSC Adv.* 5(54):43733–43740. doi:10.1039/c5ra03083h.
- Mahajan A, Arya A, Chundawat TS. 2019. Green synthesis of silver nanoparticles using green alga (*Chlorella vulgaris*) and its application for synthesis of quinoline derivatives. *Synth. Commun.* 49(15):1926–1937. doi:10.1080/00397911.2019.1610776.
- Mahdieh M, Zolanvari A, Azimee AS, Mahdieh M. 2012. Green biosynthesis of silver nanoparticles by *Spirulina platensis*. *Sci. Iran.* 19(3):926–929. doi:10.1016/j.scient.2012.01.010.
- Mikhailova EO. 2020. Silver nanoparticles: Mechanism of action and probable Bio-Application. *J. Funct. Biomater.* 11(4):84. doi:10.3390/jfb11040084.
- Mondek J, Kalina M, Simulescu V, Pekař M. 2015. Thermal degradation of high molar mass hyaluronan in solution and in powder; comparison with BSA. *Polym. Degrad. Stab.* 120:107–113. doi:10.1016/j.polymdegradstab.2015.06.012.
- More PR, Zannella C, Folliero V, Foglia F, Troisi R, Vergara A, Franci G, De Filippis A, Galdiero M. 2022. Antimicrobial applications of green synthesized bimetallic nanoparticles from *Ocimum basilicum*. *Pharmaceutics* 14(11):2457. doi:10.3390/pharmaceutics14112457.
- Murugan K, Senthilkumar B, Senbagam D, Al-Sohaibani S. 2014. Biosynthesis of silver nanoparticles using *Acacia leucophloea* extract and their antibacterial activity. *Int. J. Nanomedicine* 9:2431–2438. doi:10.2147/IJN.S61779.
- Namvar F, Azizi S, Rahman HS, Mohamad R, Rasedee A, Soltani M, Rahim RA. 2016. Green synthesis, characterization, and anticancer activity of hyaluronan/zinc oxide nanocomposite. *Onco. Targets. Ther.* 9:4549–4559. doi:10.2147/OTT.S95962.
- Pandian AMK, Karthikeyan C, Rajasimman M, Dinesh MG. 2015. Synthesis of silver nanoparticle and its application. *Ecotoxicol. Environ. Saf.* 121:211–217. doi:10.1016/j.ecoenv.2015.03.039.
- Rashad S, El-Chaghaby GA, Elchaghaby MA. 2019. Antibacterial activity of silver nanoparticles biosynthesized using *Spirulina platensis* microalgae extract against oral pathogens. *Egypt. J. Aquat. Biol. Fish.* 23(5 Special Issue):261–266. doi:10.21608/ejabf.2019.65907.
- Saha P, Mahiuddin M, Islam AB, Ochiai B. 2021. Biogenic synthesis and catalytic efficacy of silver nanoparticles based on peel extracts of *Citrus macroptera* fruit. *ACS Omega* 6(28):18260–18268. doi:10.1021/acsomega.1c02149.
- Salgin S, Salgin U, Vatanserver Ö. 2017. Synthesis and characterization of β -Cyclodextrin nanosponge and its application for the removal of p-Nitrophenol from water. *Clean - Soil, Air, Water* 45(10):1500837. doi:10.1002/clen.201500837.
- Sharifi-Rad M, Elshafie HS, Pohl P. 2024. Green synthesis of silver nanoparticles (AgNPs) by *Lallemantia royleana* leaf Extract: Their Bio-Pharmaceutical and catalytic properties. *J. Photochem. Photobiol. A Chem.* 448:115318. doi:10.1016/j.jphotochem.2023.115318.
- Shuai F, Zhang Y, Yin Y, Zhao H, Han X. 2021. Fabrication of an injectable iron (III) crosslinked alginate-hyaluronic acid hydrogel with shear-thinning and antimicrobial activities. *Carbohydr. Polym.* 260:117777. doi:10.1016/j.carbpol.2021.117777.
- Singh T, Shukla S, Kumar P, Wahla V, Bajpai VK. 2017. Application of nanotechnology in food science: Perception and overview. *Front. Microbiol.* 8:1501. doi:10.3389/fmicb.2017.01501.
- Sravani AN, Chandrasekaran N, Thomas J, Mukherjee A. 2023. Formulation and characterization of cisplatin-loaded hydroxyl functionalized single-walled carbon nanotubes for targeting gastric cancer stem cells. *Heliyon* 9(8):e18798. doi:10.1016/j.heliyon.2023.e18798.
- Traiwatcharanon P, Timsorn K, Wongchoosuk C. 2015. Effect of pH on the green synthesis of silver nanoparticles through reduction with *Pistiastratiotes* L. extract. *Adv. Mater. Res.* 1131:223–226. doi:10.4028/www.scientific.net/amr.1131.223.
- Vadakkan K, Rumjit NP, Ngangbam AK, Vijayanand S, Nedumpillil NK. 2024. Novel advancements in the sustainable green synthesis approach of silver nanoparticles (AgNPs) for antibacterial therapeutic applications. *Coord. Chem. Rev.* 499:215528. doi:10.1016/j.ccr.2023.215528.
- Ying S, Guan Z, Ofoegbu PC, Clubb P, Rico C, He F, Hong J. 2022. Green synthesis of nanoparticles: Current developments and limitations. *Environ. Technol. Innov.* 26:102336. doi:10.1016/j.eti.2022.102336.

- Yu J, Cheng L, Jia Z, Han X, Xu H, Jiang J. 2022. Injectable methylcellulose and hyaluronic acid hydrogel containing silver nanoparticles for their effective anti-microbial and wound healing activity after fracture surgery. *J. Polym. Environ.* 30(4):1330–1343. doi:10.1007/s10924-021-02257-5.
- Zamboni F, Wong CK, Collins MN. 2023. Hyaluronic acid association with bacterial, fungal and viral infections: Can hyaluronic acid be used as an antimicrobial polymer for biomedical and pharmaceutical applications? *Bioact. Mater.* 19:458–473. doi:10.1016/j.bioactmat.2022.04.023.
- Zhang X, Yao M, Chen M, Li L, Dong C, Hou Y, Zhao H, Jia B, Wang F. 2016. Hyaluronic acid-coated silver nanoparticles as a nanoplatfrom for *in vivo* imaging applications. *ACS Appl. Mater. Interfaces* 8(39):25650–25653. doi:10.1021/acsami.6b08166.